Development of a cryogenic remote sensing thermometer for CMB polarization experiment

Y. Sakurai [1], T. Matsumura[1], N. Katayama[1], H. Kanai[2], T. Iida[3]

[1] *Kavli Institute for the Physics and Mathematics of the Universe, The University of Tokyo, 5-1-5 Kashiwanoha, Kashiwa, Chiba, 277-8583, Japan*
[2] *Yokohama National University 79-1 Tokiwadai, Hodogaya-ku, Yokohama 240-8501 JAPAN*
[3] *ispace, inc. Iikurakatamachi Annex Bldg. 6F 3-1-6 Azabudai, Minato-ku, Tokyo, Japan 106-0041*
*Contact: yuki.sakurai@ipmu.jp

Abstract—**We present about the remote sensing thermometer working at cryogenic temperature for a polarization modulator used in cosmic microwave background (CMB) polarization experiment. The polarization modulator employs a superconducting magnetic bearing (SMB) in order to realize a continuous rotation at cryogenic temperature with minimal heat dissipation. The cryogenic remote thermometer is a critical development item in the polarization modulator in order to measure cryogenic, contactless and spinning rotor. We propose a novel idea to take an advantage of a temperature dependent nature in NdFeB permanent magnet. The remnance of the NdFeB peaks about 100 K and decrease as its temperature becomes lower. A simple implementation of a cryogenic Hall sensor at a vicinity of the NdFeB enables to construct a cryogenic remote temperature sensor. We calibrated the thermometer using small NdFeB magnet and applied it to a $\Phi \sim 400$ mm SMB prototype system in a 4 K cryostat with GM cooler. The obtained temperature value is good agreement with the resistive thermometer and the accuracy is ± 0.4 K in the range from 4 K to 20 K. The results are good enough to use in the polarization modulator.**

I. Introduction

One of the most important research topics in current cosmology and high-energy physics is to study the cosmic inflation theory [1,2]. The theory predicts a rapid expansion of the universe after ~10-38 seconds from the beginning of the universe. The inflation theory predicts that primordial gravitational waves from the cosmic inflation left the characteristic pattern, called B-mode, in a polarization component of a cosmic microwave background (CMB). We can still measure the CMB in microwave range as the oldest light from the big bang. Therefore, the experimental verification of the inflation theory is possible by the precise measurement of the CMB polarization signal. In order to verify the inflation theory, there are many CMB polarization experiments on the ground, balloon, and satellite. The development of related technologies is advancing innovatively.

Since the CMB polarization signal is very weak compared with the intensity signal, we need some dedicated devices or strategies for the precise measurement. A polarization modulator is one of the important instruments to realize the precise measurement [3-7]. It consists of an optical element, a half-wave plate (HWP), and a mechanism that rotates it continuously. The polarization modulator is installed at an aperture of a telescope, and it modulates an incident polarization signal. The modulation is able to reduce the impact of $1/f$ noise to the detectors and to mitigate the systematic uncertainties due to the detector differential characteristics. The HWP has to be maintained at the cryogenic temperature, e.g. below 10 K, in order to reduce noise due to its thermal emission. Therefore, the polarization modulator is required to realize a continuous rotation at cryogenic temperature with minimal heat dissipation.

A general contact type bearing, e.g. a ball bearing, makes a large heat dissipation due to the physical friction. Thus, the polarization modulator often employs a superconducting magnetic bearing (SMB) [8-9] in order to satisfy this stringent requirement. The SMB is contact-less levitation type bearing, which consists of a permanent magnet as a rotor and a superconductor array as a stator. It is possible to realize a contact-less continuous rotation at cryogenic temperature by combining the SMB with a synchronous motor, consisting of rotor permanent magnets and stator coils. The fundamental problem of the SMB is that it is hard to measure the temperature of the levitating and spinning rotor at the cryogenic environment. The temperature is crucial information to estimate the thermal loading from the HWP.

In this paper, we discuss the measurement method of the SMB rotor temperature at cryogenic temperature. We propose a novel idea to take an advantage of a temperature dependent nature in NdFeB permanent magnet. First, we calibrated the thermometer using a calibration setup with small magnets. Then, we evaluated the thermometer performance with a $\Phi \sim 400$ mm SMB prototype system in a 4 K cryostat. Finally, we discuss our results, further challenges, and how to adapt to actual experiments.

II. Cryogenic remote sensing thermometers

The infrared radiation thermometer is widely used in the various application as a remote sensing thermometer. It measures an intensity of an infrared radiation emitted from an object. The intensity is translated to the object temperature. The

infrared radiation from the rotor below 10K is significantly weak compared with room temperature. Thus, the detector of the thermometer has to be maintained in sub-Kelvin temperature for this application in order to ensure the sufficient sensitivity. However, installing a dedicated sun-Kelvin cooler for only this thermometer is not realistic.

As another proposal for remote sensing thermometer, we can consider a method of converting a physical wire to inductive contact. In this case, we can use a usual resistive thermometer for the temperature detection. As the readout of the resistive thermometer, an inductor is mounted on the spinning rotor. Another inductor or a SQUID sensor with bias current is mounted on the stator side. We can measure the induced electromotive force by mutual induction of the two inductors. Then, the obtained resistance is translated to the rotor temperature. This method has an advantage that the existing resistive thermometer can be used. However, it is necessary to make the distance of the two inductors as an order of a few μm in order to ensure the sufficient sensitivity. Thus, this method has a significant risk of a physical collision between a rotor and a stator.

The third method is to use a property of a NdFeB permanent magnet. The magnetic field of the NdFeB magnet has strong temperature dependence, especially at cryogenic temperature. Thus, it can be used as cryogenic remote sensing thermometer by installing NdFeB magnet on the rotor and measuring its magnetic field with a Hall sensor. This thermometer is suitable for the polarization modulator because the permanent magnet is already used as a rotor in the SMB.

In this paper, we focus on the third method, i.e. the permanent magnet (PM) thermometer. We describe the calibration method and the verification of the thermometer accuracy.
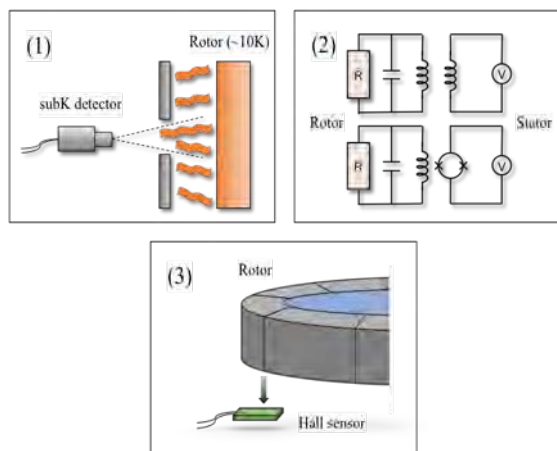

Fig. 1. The conceptual diagrams of (1) the infrared thermometer, (2) the inductive contact thermometer and (3) the permanent magnet (PM) thermometer.

III. EXPERIMENTAL SETUP

We constructed two type of experimental setup, i.e. a calibration setup and an application setup using a $\Phi \sim 400$ mm SMB. We install these setups to each dedicated 4 K cryostat with a Gifford-McMahon (GM) cooler in order to maintain an environment below 10 K. The purpose of the calibration setup is to measure the magnetic field of the permanent magnet in the temperature range from room temperature to around 4 K. We prepared two kinds of permanent magnets, NdFeB (N52) and SmCo (R33H), manufactured by Shinetsu Magnet Inc. [10]. They are small pieces of 15 mm ×15 mm × 5 mm without surface treatment. One of the magnets is mounted on an aluminum jig, as shown in Fig. 2. A cryogenic Hall sensor (HGT-3010, Lakeshore [11]) and a resistive thermometer (CX-1010, Lakeshore [12]) are installed neat the magnet. The whole setup is installed in the 4 K cryostat with the most inner shell size of 350 mm × 350 mm × 130 mm. We monitored the
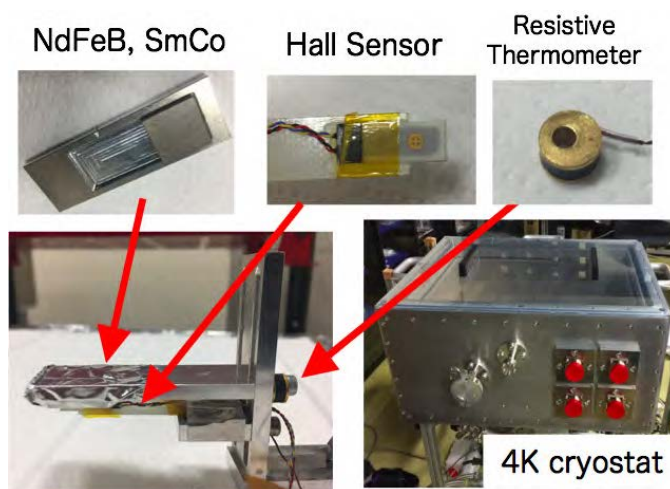

Fig. 2. The experimental setup to measure the temperature dependence of the magnetic field of the permanent magnet. The small piece (15 mm × 15 mm × 5 mm) of the permanent magnet (NdFeB or SmCo) is mounted on the aluminum jig. The Hall sensor and the resistive thermometer are attached near the magnet. The setup is installed in the 4 K cryostat with GM cooler. The 4 K shell size of this cryostat is 350 mm × 350 mm × 130 mm.

magnetic field and the temperature of the permanent magnet with different distances of 1, 2, and 3mm from the magnet surface.

We conducted the $\Phi \sim 400$ mm SMB prototype [13-15] in order to evaluate the developed PM thermometer, as shown in Fig. 3. The SMB consists of a NdFeB permanent magnet as a rotor and a YBCO superconductor array as a stator. The magnet is formed into a ring shape with 16 segmented NdFeB magnets, assembling by a coating glass epoxy. The superconductor array is also formed into a ring shape with 20 three-seeded YBCO tiles, which is covered by a glass epoxy holder. Both the magnet and the superconductor are fabricated and assembled by ATZ [16]. The SMB system is installed in $\Phi \sim 1$ m 4 K cryostat with the GM cooler. The most inner shell diameter is $\Phi = 850$ mm. The cryogenic Hall sensor is installed on top side of the rotor in order to measure the magnetic field of the rotor magnet. The resistive thermometer and heater are mounted on the surface of

the rotor magnet. The temperature of the levitating rotor is controlled by the resistive heater. It is monitored by the resistive thermometer. The resistive thermometer and heater are connected with readout wires. Therefore, the rotor is not able to be spinning with this setup. In this setup, the PM thermometer consists of the installed cryogenic Hall sensor and the SMB
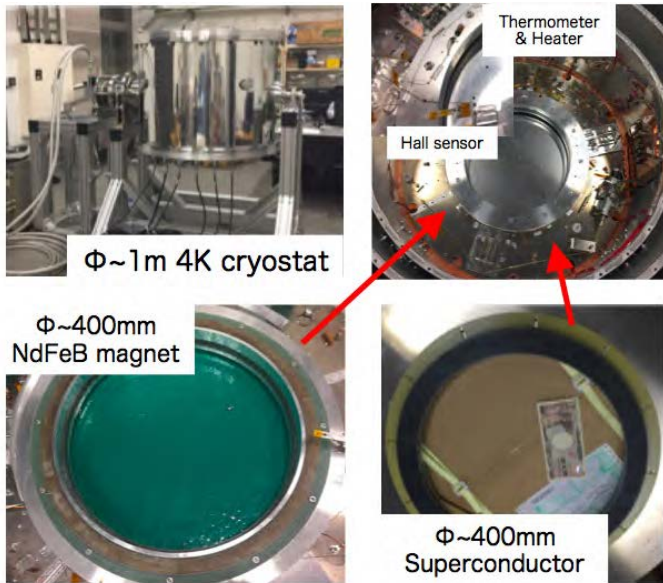

Fig. 3. The configuration of the $\Phi \sim 400$ mm SMB system. The top left picture shows the $\Phi \sim 1$ m 4 K cryostat. The top right picture shows after installing the SMB with the Hall sensor, the resistive thermometer and heater. The bottom pictures show the NdFeB rotor magnet and the YBCO superconductor array. The inner diameter of the magnet is ~ 400 mm and it consists of 16 segmented magnets with assembling by coating a glass epoxy. The superconductor array consists of 20 YBCO tiles and it is covered by a glass epoxy.

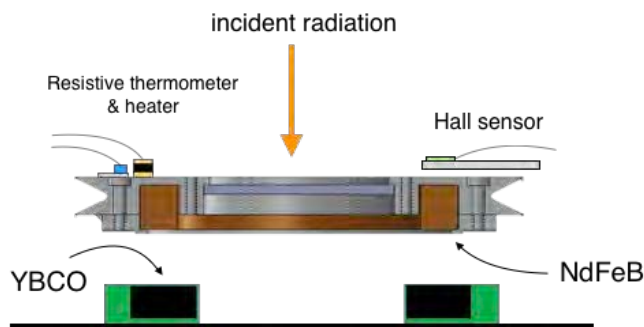rotor magnet It is evaluated by comparing with the resistive

Fig. 4. The experimental configuration to evaluate the PM thermometer. The cryogenic Hall sensor is installed top side of the levitating rotor. The resistive thermometer and heater is mounted on the surface of the levitating rotor. The rotor temperature monitored by the resistive thermometer, and it is controlled by the resistive heater. The PM thermometer consisting of the rotor magnet and the Hall sensor is evaluated by comparing with the resistive thermometer.

thermometer. The conceptual design of the experimental configuration is shown in Fig. 4.

IV. RESULTS AND THERMOMETER PERFORMANCE

A. Calibration

A magnetic field from a permanent magnet has a cryogenic temperature dependence, which differs according to kinds of permanent magnets. We measure the dependence using the calibration setup, as shown in Fig. 2. In the application of the SMB, a rare earth magnet, e.g. NdFeB or SmCo, is often used taking the advantage of their strength of the magnetic field. Other magnets have risks in the cryogenic environment due to their low-temperature demagnetization and brittleness. Thus, the temperature dependences of the NdFeB and the SmCo magnets are measured as the representative permanent magnets.
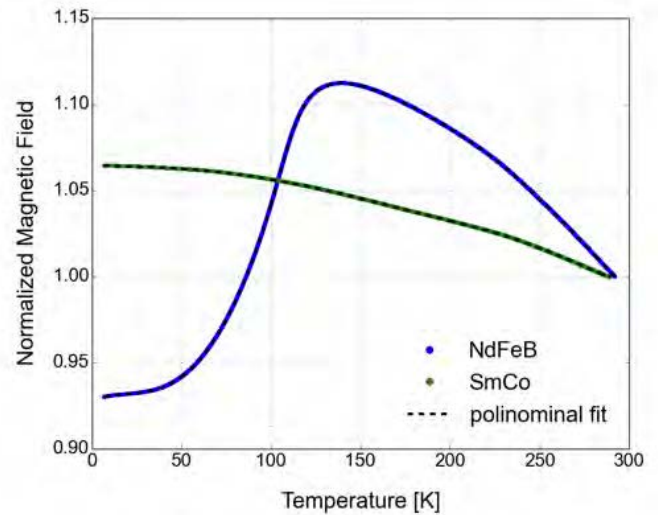

Fig. 5. The temperature dependence of the magnetic field of the permanent magnet. The blue and green lines show NdFeB and SmCo permanent magnet, respectively. The dot lines show the result of the 10th polynomial fit. The vertical axis is normalized to the absolute values of the magnetic field of room temperature (290 K).

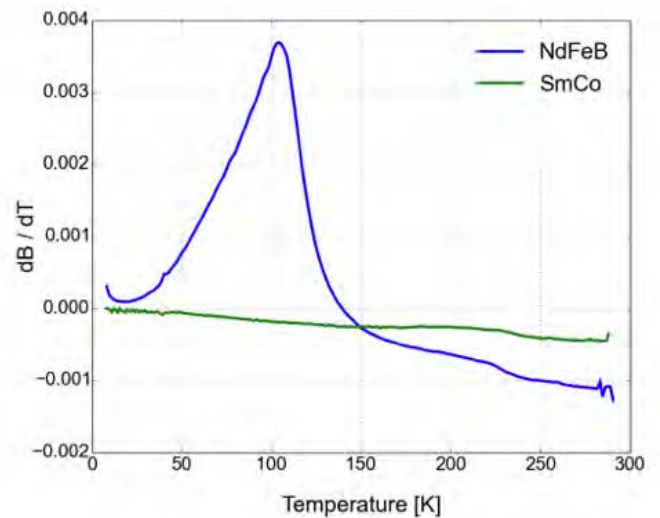Fig 5 shows the measurement result of the magnetic field with

Fig. 6. The gradient of the temperature dependence of the magnetic field from the permanent magnet. The blue and green lines show NdFeB and SmCo permanent magnet, respectively. The vertical axis represents the differential value of Fig. 5.

respect to the rotor temperature for the NdFeB and the SmCo magnets. The gradient of the measured dependence is shown in Fig 6.

From the thermometer point of view, the accuracy depends on the gradient of the variation of the magnetic field. Thus, the NdFeB magnet is suitable to use as PM thermometer compared with the SmCo magnet, as shown in Fig. 6. We use the measured shape of the Fig. 5 as the calibration curve of the PM
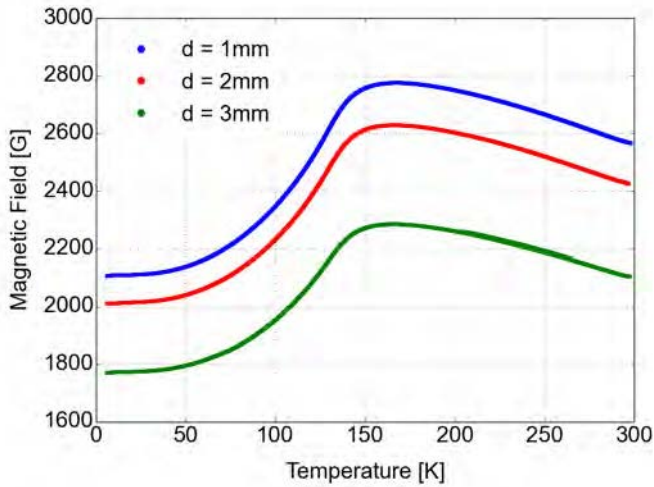

Fig. 7. The temperature dependence of the magnetic field from the permanent magnet with different distances between the Hall sensor and the surface of the magnet. The blue, red and green lines represents the distance is 1, 2 and 3mm, respectively.

thermometer. Once we measure the magnetic field of the NdFeB magnet, we can translate it to the temperature of the magnet. However, the strength of the measured magnetic field follows the distance between the Hall sensor and the permanent magnet. Thus, we also measured the temperature dependence with different distances of 1, 2 and 3 mm, as shown in Fig. 7.

B. Spin reorientation transition of NdFeB

The characteristic shape of the NdFeB magnet in Fig. 5 is known as a spin reorientation transition (SRT) [17-20]. The SRT represents a change of the magnetization direction toward the energy stable state in a crystal. The conceptual diagram of the SRT is shown in Fig. 8. The transition temperature of the NdFeB magnet is known as around 135 K. From the room temperature to the transition temperature, the NdFeB magnetic spin prefers the direction along the c-axis of its tetragonal crystal, i.e. an easy-axis. Below the transition temperature, this spin direction is away from the easy-axis by the canting angle θ, which depends on the magnet temperature. The maximum deviation of the angle is 30 degrees at 4.2 K. The cone defined by θ is referred as an easy-cone. The magnetization direction is tiled by the SRT, and the installed cryogenic Hall sensor is sensitive to the vertical magnetic field. Therefore, the magnetic field rapidly decreases below the transition temperature. The SRT is due to the complex tetragonal crystal structure and the unusual combination of the magnetic anisotropy.
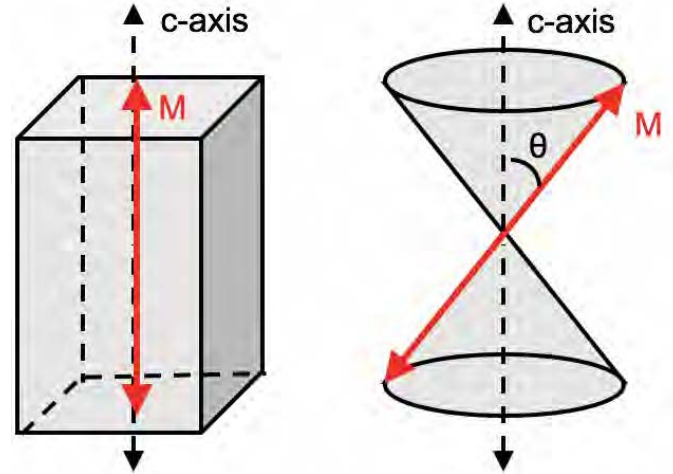

Fig. 8. The conceptual design of the preferred magnetization direction. Above the transition temperature, the magnetization direction, M, is aligned to c-axis in the crystal. Below the transition temperature, M is aligned on the cone surface away from the c-axis at the angle of **θ**.

C. Performance test using the SMB prototype

We apply the developed PM thermometer to the $\Phi \sim 400$ mm SMB prototype. The experimental configuration is shown in Fig. 4. The SMB system is cooled down to around 4 K. We prepare a space of 5 mm between the rotor magnet and the YBCO stator as a levitation height. After the cooling, the rotor is released by the cryogenic actuators. The rotor is levitated by a Meissner effect and the position is fixed by a pinning effect of the type II superconductor. The rotor is slightly dropped from the initial levitation height due to a gravity effect. The dropping distance is estimated by the reduction rate of the magnetic field with respect to the distance between the rotor magnet and the
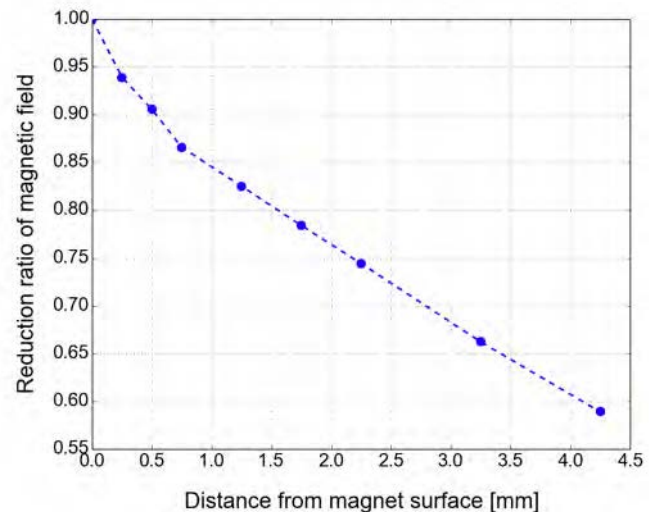

Fig. 9. The reduction ratio of the magnetic field with respect to the distance from the magnetic surface, obtained from the electromagnetic simulation.

cryogenic Hall sensor. Fig. 9 shows the reduction rate obtained by a static electromagnetic simulation [21].

There is no thermal contact with levitating rotor except for the wires of the resistive thermometer and heater. The rotor temperature is increased by the resistive heater by applying a certain voltage and inputting the Joule heat. In order to cool the rotor, the rotor is re-gripped by the cryogenic actuators. During this increasing and cooling cycle of the rotor temperature, we continue to monitor both output signals from the resistive thermometer and from the Hall sensor as the PM thermometer.

The measured magnetic field is translated to the temperature using the calibration curve considering the dropping distance. Then, we evaluate the PM thermometer by comparing with the resistive thermometer. Fig. 10 shows the obtained temperatures
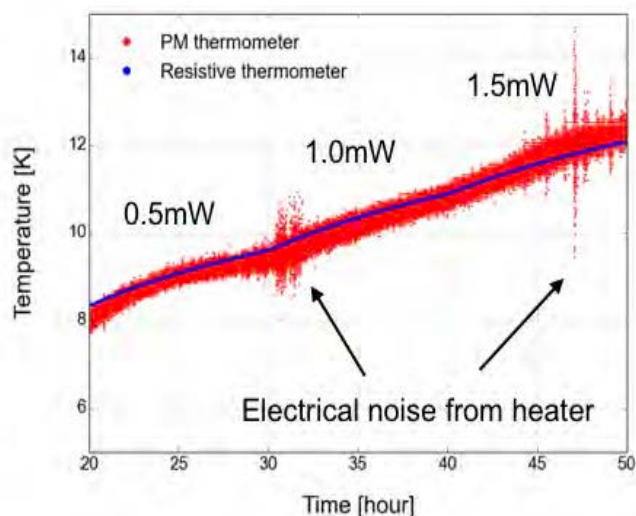

Fig. 9. The comparison of the temperature from the resistive thermometer (blue) and the PM thermometer (red). The levitating rotor is heated by the resistive heater with different input power of 0.5, 1.0 and 1.5 mW.
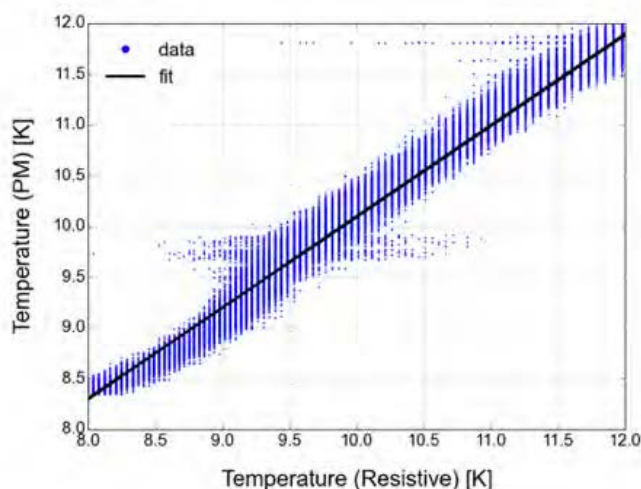

Fig. 10. The linearity between the resistive and the PM thermometer. The blue dot shows the obtained data and the solid line shows a linear fit of the data.

from the resistive thermometer and from the PM thermometer as a function of time. The levitating rotor is gradually heated by biasing the resistive heater with different input powers of 0.5, 1.0 and 1.5 mW. There is a good agreement between two thermometers. The spikes in the PM thermometer output are due to the electrical noise changing the bias voltage. The linearity between the resistive and the PM thermometer is shown in Fig. 11. The temperature accuracy of the PM thermometer in the range from 4 K to 20 K is $\pm$ 0.4 K, which is defined by the standard deviation of the temperature variation.

V. DISCUSSIONS

We demonstrated the performance of the PM thermometer using the SMB prototype. The temperatures from resistive thermometer and from the PM thermometer were consistent. The accuracy of the PM thermometer was calculated from the result. In this setup, the wires are connected to the resistive thermometer on the rotor. Thus, it is not possible to measure the rotor temperature during rotation. In order to adapt to the actual modulator, it is necessary to consider the effect of the magnetic field variation during rotation. There is a specific pattern in the magnetic field variation due to the segmented ring magnet in one rotation [18]. Thus, the average value of the variation can be used as the argument of the calibration function.

In addition, the displacement of the rotor magnet in vertical axis due to gravity effect has to be considered. Since the calibration curve can be normalized by the distance between the rotor magnet and the Hall sensor, the displacement can be treated as the vertical geometry factor in the calibration curve.

Therefore, the output of the PM thermometer, *T,* can be represented as

$$T = F\left(\frac{1}{n}\sum_{0 \leq \theta \leq 2\pi}^{n} B_\theta , G_Z\right), \qquad (1)$$

where F is the calibration function as shown is Fig. 5. B_θ is the measured magnetic field at angle θ, and n is the number of measurement points. θ can be reconstructed by an optical encoder. G_Z is the geometry factor in vertical direction?

From the SMB performance point of view, the SmCo has an advantage to use as the rotor magnet compared to the NdFeB. In case of the NdFeB, the magnetic field pinned to the YBCO at the transition temperature of 94 K and the magnetic field of the rotor magnet below 10 K are about 10 % different. Thus, the SmCo which has less temperature dependence is suitable for the SMB. In this case, the rotor magnet is not able to use as the PM thermometer. However, it is sufficient for the PM thermometer to mount the small piece of the NdFeB magnet on top of the rotor, with installing the Hall sensor close to it. Since the measured magnetic fields are averaged as equation (1), the effect of the rotation is able to be ignored. The demonstration of this method will be followed up by future papers.

CONCLUSIONS

We proposed and developed the PM thermometer as the cryogenic remote sensing thermometer for the polarization modulator used in CMB polarization experiments. We measured the calibration curve between the magnetic field and the temperature using the small piece of the NdFeB magnet and the cryogenic Hall sensor. We confirmed that the characteristic dependence due to the spin reorientation transition of the NdFeB magnet. The calibrated PM thermometer is evaluated using the $\Phi \sim 400$ mm SMB prototype comparing with the temperature from the resistive thermometer. We obtained the consistent result between the PM thermometer and the resistive thermometer. The temperature accuracy of the PM thermometer is $\pm$ 0.4 K, which is sufficient for the actual application. We discussed that how to actually adapt the PM thermometer to the SMB of the polarization modulator. The spinning effect and the distance relationship between the magnet and the Hall sensor can be treated by using the average and the geometry factors. Therefore, we successfully developed the cryogenic remote sensing thermometer which is applicable to the SMB of the polarization modulator.

ACKNOWLEDGMENT

REFERENCES

[1] K. Sato, "First-order phase transition of a vacuum and the expansion of the Universe", Monthly Notices of Royal Astronomical Society, 195, 467, (1981).

[2] H. Guth Alan, "The Inflationary Universe: A Possible Solution to the Horizon and Flatness Problems", Phys. Rev. D 23, 347 (1981).

[3] J. H. P. Wua, J. Zuntz, M. E. Abroe, P. A. R. Ade, J. Bock, J. Borrill, J. Collins, S. Hanany, A. H. Jaffe, B. R. Johnson, T. Jones, A. T. Lee, T. Matsumura, B. Rabii, T. Renbarger, P. L. Richards, G. F. Smoot, R. Stompor, H. T. Tran, and C. D. Winant, "MAXIPOL: data analysis and results," The Astrophysical Journal 665, 55 (2007).

[4] Britt Reichborn-Kjennerud, Asad M. Aboobaker, Peter Ade, Françcois Aubin, Carlo Baccigalupi, Chaoyun Bao, Julian Borrill, Christopher Cantalupo, Daniel Chapman, Joy Didier, Matt Dobbs, Julien Grain, William Grainger, Shaul Hanany, Seth Hillbrand, Johannes Hubmayr, Andrew Jaffe, Bradley Johnson, Terry Jones, Theodore Kisner, Jeff Klein, Andrei Korotkov, Sam Leach, Adrian Lee, Lorne Levinson, Michele Limon, Kevin MacDermid, Tomotake Matsumura, Xiaofan Meng, Amber Miller, Michael Milligan, Enzo Pascale, Daniel Polsgrove, Nicolas Ponthieu, Kate Raach, Ilan Sagiv, Graeme Smecher, Federico Stivoli, Radek Stompor, Huan Tran, Matthieu Tristram, Gregory S. Tucker, Yury Vinokurov, Amit Yadav, Matias Zaldarriaga, Kyle Zilic, "EBEX: a balloon-borne CMB polarization experiment," Proc. SPIE 7741, 77411C (2010)

[5] T. E. Montroy, P. A. R. Ade, R. Bihary, J. J. Bock, J. R. Bond, J. Brevick, C. R. Contaldi, B. P. Crill, A. Crites, O. Doré, L. Duband, S. R. Golwala, M. Halpern, G. Hilton, W. Holmes, V. V. Hristov, K. \ Irwin, W. C. Jones, C. L. Kuo, A. E. Lange, C. J. MacTavish, P. Mason, J. Mulder, C. B.

Netterfield, E. Pascale, J. E. Ruhl, A. Trangsrud, C. Tucker, A. Turner, M. Viero, "SPIDER: a new balloon-borne experiment to measure CMB polarization on large angular scales," Proc. SPIE 6267, 62670R (2006).

[6] A. Kusaka, T. Essinger-Hileman, J. W. Appel, P. Gallardo, K. D. Irwin, N. Jarosik, M. R. Nolta, L. A. Page, L. P. Parker, S. Raghunathan, J. L. Sievers, S. M. Simon, S. T. Staggs, K. Visnjic, "Modulation of cosmic microwave background polarization with a warm rapidly rotating half-wave plate on the Atacama B-Mode Search instrument," Review of Scientific Instruments 85, 024501 (2014)

[7] Charles A. Hill, Shawn Beckman, Yuji Chinone, Neil Goeckner-Wald, Masashi Hazumi, Brian Keating, Akito Kusaka, Adrian T. Lee, Frederick Matsuda, Richard Plambeck, Aritoki Suzuki, Satoru Takakura, "Design and development of an ambient-temperature continuously-rotating achromatic half-wave plate for CMB polarization modulation on the POLARBEAR-2 experiment", Proc.SPIE Int.Soc.Opt.Eng. 9914 (2016) 99142U (2016)

[8] J. Hull, "Topical review: Superconducting bearings, Superconductor Science", 110, 140, Technology 13 (1).

[9] Jeff Klein, Asad Aboobaker, Peter Ade, François Aubin, Carlo Baccigalupi, Chaoyun Bao, Julian Borrill, Daniel Chapman, Joy Didier, Matt Dobbs, Benjamin Gold, Will Grainger, Shaul Hanany, Johannes Hubmayr, Seth Hillbrand, Julien Grain, Andrew Jaffe, Bradley Johnson, Terry Jones, Theodore Kisner, Andrei Korotkov, Sam Leach, Adrian Lee, Lorne Levinson, Michele Limon, Kevin MacDermid, Tomotake Matsumura, Amber Miller, Michael Milligan, Enzo Pascale, Daniel Polsgrove, Nicolas Ponthieu, Kate Raach, Britt Reichborn-Kjennerud, Ilan Sagiv, Radek Stompor, Huan Tran, Matthieu Tristram, Gregory S. Tucker, Amit Yadav, Matias Zaldarriaga, Kyle Zilic, "A cryogenic half-wave plate polarimeter using a superconducting magnetic bearing", Proceedings of the SPIE, Cryogenic Optical Systems and Instruments XIII, Volume 8150, 815004 (2011).

[10] Shinetsu Magnet Inc., Japan. [Online]. Available: www.shinetsu-rare-earth-magnet.jp/e/ . Accessed on: Jun. 1, 2018.

[11] Lakeshore, USA. [Online] Available: www.lakeshore.com/products/Hall-Magnetic-Sensors/Pages/Specifications.aspx . Accessed on: Jun. 1, 2018

[12] Lakeshore,USA.[Online]Available: www.lakeshore.com/products/Cryogenic-Temperature-Sensors/Cernox/Models/Pages/Specifications.aspx. Accessed on: Jun. 1, 2018.

[13] T. Matsumura, H. Kataza, S. Utsunomiya, R. Yamamoto, M. Hazumi, N . Katayama, "Design and Performance of a Prototype Polarization Modul ator Rotational System for Use in Space Using a Superconducting Magn etic Bearing", IEEE Transactions on Applied Superconductivity, Volum e: 26, Issue 3, (2016).

[14] Y. Sakurai, T. Matsumura, H. Kataza, S. Utsunomiya, R. Yamamoto, "E stimation of the heat dissipation and the rotor temperature of supercondu cting magnetic bearing below 10 K", IEEE Transactions on Applied Sup erconductivity, Vol. 27, Iss. 4 (2017).

[15] Y. Sakurai, T. Matsumura, H. Sugai, N. Katayama, H. Ohsaki, Y. Terao, Y. Terachi, H. Kataza, S. Utsunomiya, and R. Yamamoto, "Vibrational c haracteristics of a superconducting magnetic bearing employed for a prot otype polarization modulator", J. Phys.: Conf. Ser. 871, 012091 (2017).

[16] Adelwitz Technologiezentrum GmbH (ATZ), Germany. [Online]. Avail able: www.atz-gmbh.com. Accessed on: Jun. 1, 2018.

[17] J. F. Herbst. R2Fe14B materials: Intrinsic properties and technological a spects. Reviews of Modern Physics, 63(4):819–898, 1991.

[18] J. F. Herbst, J. J. Croat, F. E. Pinkerton, and W. B. Yelon. Relationships between crystal structure and magnetic properties in Nd2Fe14B. Physica l Review B, 29(7):4176–4178, 1984.

[19] D. Givord, H.S. Li, and J.M. Moreau. Magnetic properties and crystal str ucture of Nd2Fe14B. Solid State Communications, 50(6):497–499, 1984 .

[20] Stanley R. Trout, Using Permanent Magnets at Low Temperatures. TN 0 302 p.1 June 2003.

[21] Y. Terachi, H. Ohsaki, Y. Terao, Y. Sakurai, T. Matsumura, H. Sugai, S. Utsunomiya, H. Kataza and R. Yamamoto: "Numerical Analysis of Fun damental Characteristics of Superconducting Magnetic Bearings for a Po larization Modulator," IOP Publishing, Journal of Physics Conference Se ries, Vol. 871. No. 1, p.012094, 2017.